INORGANIC CHEMISTRY FRONTIERS

RESEARCH ARTICLE

View Article Online
View Journal | View Issue

Cite this: *Inorg. Chem. Front.*, 2024, **11**, 2436

Durable dielectric switching and photo-responsivity in a Dion–Jacobson hybrid perovskite semiconductor†

Peng Wang,[a,b] Xinling Li,[a,b] Huang Ye,[b,d] Qianwen Guan,[b,d] Yifei Wang,[b,d] Yaru Geng,[b] Chengshu Zhang,[b,d] Hang Li[b,d] and Junhua Luo *[a,b,c,d]

Two-dimensional hybrid perovskite (2DHPs) semiconductors have shown great potential in multifunctional applications, especially dielectric switches and photoelectric detection owing to their diverse structural feasibility and excellent semiconducting features. However, most of the reported 2DHPs belong to the Ruddlesden–Popper (R–P) type, which unavoidably suffers from weak van der Waals interactions, degrading their reliability for long-term operation. The recently developed environmentally stable Dion–Jacobson (D–J) phase perovskites provide us with an opportunity to design 2DHPs with durable working performances. Here, we report a D–J phase perovskite material (BDA)$MA_2Pb_3Br_{10}$ (**1**, where BDA^{2+} is 1,4-butanediammomium and MA^+ is methylammonium) that displays a remarkable switchable dielectric anomaly at 322 K. Meanwhile, the single crystal devices of **1** exhibit impressive photoelectric detection performances, featuring a large on/off current ratio (~6.19×10^3), remarkable responsivity (~11.79 mA W^{-1}), and high detectivity (~2.9×10^{11} Jones). Additionally, due to the phase stability conferred by the D–J structure, these devices exhibit excellent photoresponsivity and resistance to fatigue, as evidenced by over 1200 photoresponse cycles, along with noteworthy stability in dielectric switching (maintained for two months). This study presents a comprehensive methodology for designing highly stable D–J phase perovskites with exceptional performance in dielectric switching and photoelectric detection, thereby expanding the repertoire of 2D D–J multifunctional hybrid perovskites.

Received 29th December 2023,
Accepted 1st March 2024

DOI: 10.1039/d3qi02685j

rsc.li/frontiers-inorganic

Introduction

Two-dimensional hybrid perovskites (2DHPs), with their structural diversity and composition tunability, have emerged as a hotspot of research in numerous fields, including solar harvesting, photoelectric diodes, ferroelectrics, and nonlinear optics.[1–4] In particular, in the region of phase transition materials, the dynamic synergistic effect between organic and inorganic components in 2DHPs significantly facilitates the introduction of thermal-triggered ordered–disordered transitions.[5–8] This characteristic results in notable dielectric anomalies, making 2DHPs suitable for applications as thermal stimuli dielectric switching materials, offering novel capabilities such as temperature sensing, smart switching, and information processing.[9–12] Moreover, benefiting from the excellent semiconductor properties brought by the inorganic framework, including high optical absorption, defect tolerance, and long carrier lifetime, 2DHPs have also sparked great research enthusiasm in the field of photoelectric detection.[13–18] Therefore, 2DHPs are considered an ideal platform for integrating dielectric switching and photo-responsivity features, thereby promoting the development of multifunctional materials. For example, Sun *et al.* reported a series of 2DHPs that synchronously exhibited excellent photosensitivity and giant dielectric anomalies, showcasing their significant application value.[19–21] Despite these significant achievements, most reported dielectric switching 2DHPs are based on the Ruddlesden–Popper (R–P) type.[22–25] Structurally, the interlayer cations in R–P 2DHPs are loosely connected through weak van der Waals interactions, rendering them vulnerable to

[a]*College of Chemistry, Fuzhou University, Fuzhou 350116, China*
[b]*State Key Laboratory of Structure Chemistry, Fujian Institute of Research on the Structure of Matter, Chinese Academy of Sciences, Fuzhou, Fujian, 350002, P. R. China. E-mail: jhluo@fjirsm.ac.cn*
[c]*Key Laboratory of Fluorine and Silicon for Energy Materials and Chemistry of Ministry of Education, School of Chemistry and Chemical Engineering, Jiangxi Normal University, Nanchang, Jiangxi 330022, China*
[d]*University of Chinese Academy of Sciences, Beijing, 100049, China*

†Electronic supplementary information (ESI) available: Crystallographic data and experimental section. CCDC 2231790 and 2231791. For ESI and crystallographic data in CIF or other electronic format see DOI: **https://doi.org/10.1039/d3qi02685j**

long-term working conditions and limiting their practical applications.[26–28] Thus, it is of strategic and scientific significance to explore durable dielectric switching 2DHPs.

The recently developed Dion–Jacobson (D–J) hybrid perovskites provide us with an opportunity to obtain the desired materials. Unlike its R–P homolog, the introduction of diamine cations in the interlayer results in the elimination of the van der Waals gap, preventing the intervention of air and water molecules, thus improving the phase stability of the material[29,30] and largely extending its working reliability in photovoltaic applications. For example, Sajjad Ahmad *et al.* developed a series of D–J phase 2D perovskites $(PDA)(MA)_{n-1}Pb_nI_{3n+1}$ (n = 1–4), which exhibited ultrahigh device stability. The devices without encapsulation retain over 95% efficiency on exposure to harsh environments.[31] Although D–J type 2DHPs have made tremendous progress in photoelectric devices, the current research focus on D–J 2DHPs with dielectric switching features is limited. Therefore, exploration of D–J 2DHPs with dielectric switching features and high photoresponsivity is an urgent step in the development of environmentally stable multifunctional materials.

Here, we have synthesized a D–J hybrid perovskite (BDA)$MA_2Pb_3Br_{10}$ (**1**, BDA^{2+} is 1,4-butanediammomium and MA^+ is methylammonium), which exhibits reversible dielectric switching at 322 K. Furthermore, **1** exhibits excellent photo-responsivity, including a large on/off ratio of 6.19×10^3, a high detectivity of 2.9×10^{11} Jones, and a remarkable responsivity of 11.79 mA W^{-1}. Moreover, **1** exhibits excellent fatigue resistance, as demonstrated by over 1200 photoresponse cycles and outstanding dielectric switching stability (maintained for two months). This work paves the way for the design of highly stable 2D D–J perovskites with dielectric anomalies and photoelectric detection performance, enriching the family of multifunctional dielectric switches.

Results and discussion

The single crystals of **1** which are up to $20 \times 6 \times 1$ mm^3 in size are grown by the temperature-cooled solution method (Fig. S1†), and the phase purity of the sample is confirmed by the powder X-ray diffraction pattern (Fig. S2†). The quality of the crystal face is qualified using a scanning electron microscope (SEM), as shown in Fig. S3.† The image demonstrates the flat and smooth surface, indicating the high quality of the single crystal, which is beneficial for high-performance photodetection. In order to understand the structure–function relationship, single-crystal X-ray diffraction was conducted to determine the structural details of $(BDA)MA_2Pb_3Br_{10}$. As is demonstrated in Fig. 1a, **1** adopts a 2D trilayer perovskite architecture, in which the trilayer inorganic frameworks consist of corner-sharing $PbBr_6$ octahedra, and the BDA^{2+} cations are arranged in a staggered manner within the interlayer space, forming an organic–inorganic alternate quantum well structure. Such a structure is beneficial for the dissociation of photogenerated electron–hole pairs and results in a longer lifetime of free carriers, leading to an improvement in photoconductivity. For 2D R–P perovskite, the organic cations are loosely connected by weak van der Waals interactions, inhibiting long-term operation and limiting their practical application. In contrast, the diamine moieties in D–J phase perovskites are connected to the inorganic sheets by hydrogen bonds, eliminating the van der Waals gap interaction and improving the optoelectronic detection performance.[32,33]

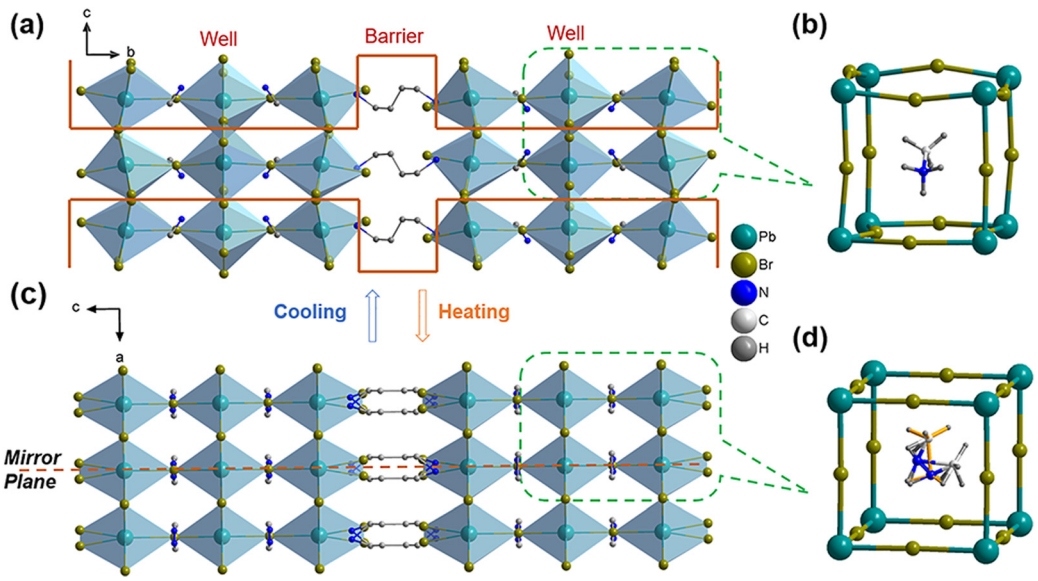

Fig. 1 (a) A schematic diagram of the quantum-well-like structure of **1** at LTP. (b) The inorganic framework, with the MA^+ cation incorporated inside the cavity at LTP. (c) Single crystal structures of **1** at HTP. (d) The inorganic framework, with the disordered MA^+ cation inside the cavity at HTP; the two folds of cations have been distinguished in different colours.

We further explore variable temperature structural analysis at the low-temperature phase (LTP) and high-temperature phase (HTP) to investigate the phase transition mechanism of **1**. At the LTP, **1** crystallizes in the *Pnma* space group (Table S1†). As is described in Fig. S4 and Tables S2 and S3,† the $PbBr_6$ octahedra show a distorted geometric configuration with an average Pb–Br–Pb bond angle of 132.78° and Pb–Br bond lengths of 2.84–3.15 Å. The coupling of the ordered organic cations (MA^+ and BDA^{2+}) and distorting Pb–Br sheets can be considered as a driving force to trigger the phase transition as the temperature increases (Fig. 1b). At the HTP, **1** crystallizes in the *Cmcm* space group (Table S1†). Both the organic cations MA^+ and BDA^{2+} become disordered and are highly symmetrical relative to the mirror plane (Fig. 1c and d). In addition, the inorganic sheets adopt a highly symmetric configuration, which is confirmed by the average Pb–Br–Pb bond angle, calculated to be 179.976° (Fig. S4 and Table S4†). It can be concluded that the order–disorder transition of the organic cations and inorganic framework is the key factor in the temperature-induced reversible phase transition, which further generates the dielectric anomaly.

In order to further investigate the reversible phase transition process of compound **1**, differential scanning calorimetry (DSC) measurement was performed and is shown in Fig. 2a, and a pair of reversible thermal peaks at 329 K and 322 K can be observed during the heating and cooling process. Meanwhile, the temperature-dependent dielectric constant test is recorded in Fig. 2b. A step-like dielectric anomaly is observed around 322 K during the heating and cooling process, consistent with the DSC results, indicating the occurrence of a reversible phase transition. Moreover, the dielectric constants at different frequencies (at 10 kHz, 100 kHz, 300 kHz, 500 kHz, and 1000 kHz) show similar dielectric anomalous behaviour during the heating processes (Fig. S5a†) and the dielectric anomaly of the *a*-axis is more significant than that of the *b*- and *c*-axes in the 1000 kHz axial directions (Fig. S5b†), evidencing the anisotropies of **1**. The fundamental optical and semiconductor characteristics are verified by the UV–visible absorption spectrum, showing a sharp optical absorption cut-off at ~550 nm. The band gap is estimated to be 2.50 eV by the *Tauc* equation. This value is comparable with those of other two-dimensional lead–bromine perovskites, such as $(BA)_2(DMA)Pb_2Br_7$ (~2.65 eV) and $BA_2EA_2Pb_3Br_{10}$ (~2.55 eV),[34,35] and is suitable for photodetection in the visible region. Furthermore, the photoluminescence (PL) of **1** is recorded with a narrow emission peak at 510 nm (Fig. S6†), indicating that the electron–phonon coupling effect of **1** is weakened, which is favorable for photoelectric detection. In addition, we performed first-principles DFT calculations to investigate the band gap of **1**, indicating that **1** is a direct bandgap semiconductor with the valence band maximum (VBM) and conduction band minimum (CBM) located at the same *k*-point G, and the band gap was calculated to be 2.540 eV, in good agreement with the experimental results. The partial density of states (PDOS) reveals the contribution of different atomic orbitals to the band gap. As shown in Fig. 3c, the VBM mainly stems from the Pb 6s and Br 4p states, while the CBM is mainly determined by the Pb 6p state. Therefore, the semiconductor properties of **1** are chiefly governed by the inorganic layers. In addition, Fig. 3d describes the temperature-dependent conductivities along the three axes (*a*-, *b*-, and *c*-). During the heating process, the curve shows an upward trend, which also indicates the semiconductor properties of **1**. In particular, the conductivity rises sharply as the temperature approaches 322 K, which agrees well with its phase transition temperature, further validating that the distortion degree of the inorganic framework in HTP is smaller than that in LTP, and the conductivity is improved. These results above reveal the excellent semiconductor properties of **1**, which provide potential for application in photodetection.

To investigate the photodetection capability of **1**, a single crystal-based bi-lateral device is shown in Fig. 4a. The dark current is measured as 4.2×10^{-10} A under a V_{bias} of 10 V. When the light intensity is 35.88 mW cm^{-2}, the photocurrent increases to a saturated I_{photo} of 2.6×10^{-6} A (Fig. 4b), and the on/off ratio is about 6.19×10^3. This value is at the same level as those of the reported two-dimensional multilayer perovskite photodetectors, such as $(i\text{-}PA)_2CsAgBiBr_7$ and $(ALA)_2(EA)_2Pb_3Br_{10}$.[36,37] Fig. 4c shows the light intensity depen-

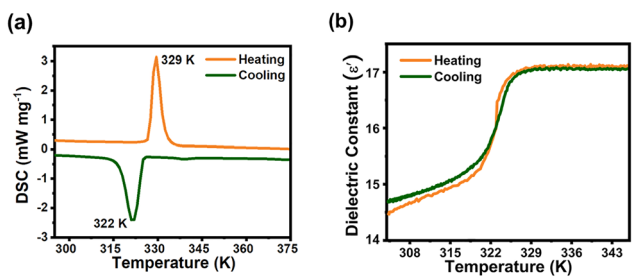

Fig. 2 (a) The DSC curve of **1** and (b) the dielectric constant curve of **1** at 1000 kHz.

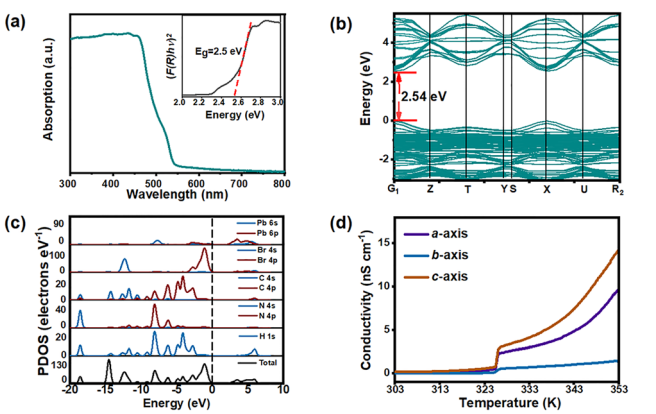

Fig. 3 (a) The UV-vis absorption spectrum of **1** (inset: the experimental bandgap). (b) The calculated bandgap diagram of **1**. (c) PDOS of **1**. (d) Variable temperature conductivity test along different axes of single crystals.

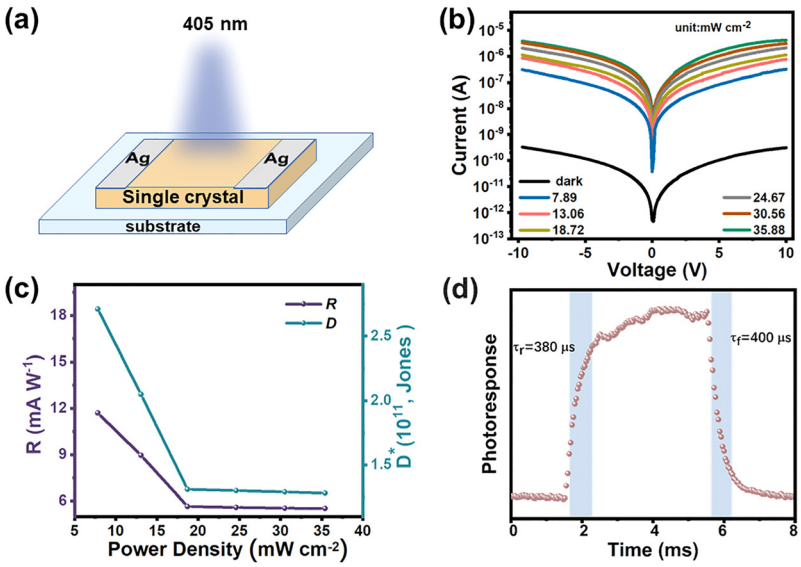

Fig. 4 (a) The photodetection device schematic diagram of **1**. (b) The *I*–*V* curves of **1** measured at 405 nm with different incidence powers. (c) *R* and *D** calculated from the photocurrent measured at 10 V bias. (d) The response time of **1**.

dent responsivity (R) and detectivity (D^*) of a single crystal device at 405 nm. And the maximum R and D^* are 11.79 mA W^{-1} and 2.9×10^{11} Jones, respectively, comparable with those of other D–J-phase hybrid perovskites, such as (3AMPY)(EA)Pb_2Br_7 and (HIS)(DMA)Pb_2Br_7.[38,39] The response time is another important parameter of photodetectors. As shown in Fig. 4d, the rise (τ_r) and decay (τ_f) photoresponse times are 380 and ~400 μs, respectively, during the switching "on–off" cycle, indicating that **1** is promising for future fast photoresponse devices.

To further explore the environmental stability and fatigue resistance, we evaluated the environmental stability of **1**, as evidenced by the PXRD patterns of **1**, which are consistent with the initial results (maintained for three months). In addition, we analyzed the thermal stability of **1** by thermogravimetric analysis (TGA), as shown in Fig. 5b. The trace of **1** starts to decompose slowly at 560 K, which is much higher than its phase transition temperature. It is noteworthy that the temperature range from the phase transition temperature to the decomposition temperature is 345 K, indicating that **1** has high thermal stability as a dielectric switch. Such high environmental stability will be suitable for various application scenarios. To further investigate the high operating stability of the device, the durability of its dielectric switching and photo-

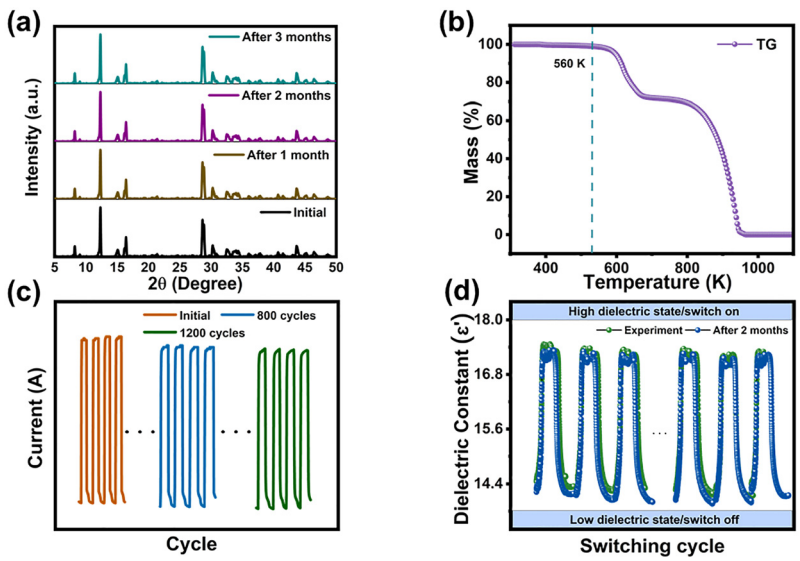

Fig. 5 (a) The phase stability of **1** by the PXRD patterns. (b) TG curve of **1**. (c) The photoresponse capability of **1** after 800 and 1200 *I*–*T* cycles at 405 nm. (d) Periodic of repeatable switching measurement after several on/off cycles at 1 MHz.

responsivity were recorded. After 800 and 1200 photoresponse cycles at 405 nm (Fig. 5c), the saturated I_{photo} remains at a relatively stable level, indicating the favourable anti-fatigue properties of **1**. Dielectric cycling stability is another important parameter of stability. As revealed in Fig. 5d, the dielectric constant value remains constant after several dielectric cycles. Importantly, the device of **1** also exhibits excellent dielectric switches after exposure to air for 2 months. These features indicate that **1** has excellent environmental stability and excellent working stability, which will further enrich its application scenarios in multifunctional responsive materials.

Conclusions

In summary, we have constructed a two-dimensional (2D) Dion–Jacobson (D–J) phase perovskite $(BDA)MA_2Pb_3Br_{10}$, which exhibits obvious dielectric anomalies along different axes at 322 K. Additionally, **1** exhibits excellent photoelectric detection performance, with a large switching ratio of 6.19×10^3, a remarkable responsivity of 11.79 mA W^{-1}, and a high detectivity of 2.9×10^{11} Jones. In particular, based on the intrinsic structural stability of the D–J phase perovskites, single crystal devices of **1** reveal excellent thermal, environmental, and operating stability. The devices of **1** possess excellent photo-responsivity antifatigue merits (over 1200 photoresponse cycles) and remarkable switching stability (maintained for two months). Our work presents a comprehensive methodology for ultra-stable optoelectronic applications and dielectric switches, which will inspire further intriguing research on multifunctional dielectric switches.

Conflicts of interest

The authors declare no conflict of interest.

Acknowledgements

This work was financially supported by the National Natural Science Foundation of China (52202194, 22193042, 21833010, 21921001, 22305105, and 22201284) and the Key Research Program of Frontier Sciences of the Chinese Academy of Sciences (ZDBSLY-SLH024).

References

1 A. Caiazzo and R. A. J. Janssen, High efficiency quasi–2D Ruddlesden–Popper perovskite solar cells, *Adv. Energy Mater.*, 2022, **12**, 2202830.
2 L. Hua, J. Wang, Y. Liu, W. Guo, Y. Ma, H. Xu, S. Han, J. Luo and Z. Sun, Improper high-Tc perovskite ferroelectric with dielectric bistability enables broadband ultraviolet-to-infrared photopyroelectric effects, *Adv. Sci.*, 2023, **10**, 2301064.
3 J.-W. Lee and N.-G. Park, Quasi-two-dimensional perovskite light emitting diodes for bright future, *Light: Sci. Appl.*, 2021, **10**, 86.
4 X. Li, Y. Guan, X. Li and Y. Fu, Stereochemically active lone pairs and nonlinear optical properties of two-dimensional multilayered tin and germanium iodide perovskites, *J. Am. Chem. Soc.*, 2022, **144**, 18030–18042.
5 Y. Liu, H. Xu, X. Liu, S. Han, W. Guo, Y. Ma, Q. Fan, X. Hu, Z. Sun and J. Luo, A room-temperature antiferroelectric in hybrid perovskite enables highly efficient energy storage at low electric fields, *Chem. Sci.*, 2022, **13**, 13499–13506.
6 C. Gao, H. Xu, W. Guo, Y. Liu, Q. Fan, Y. Ma, T. Yang, W. Li, J. Luo and Z. Sun, Light-induced dielectric enhancement in a 2D Dion–Jacobson type perovskite phase transition material, *Adv. Opt. Mater.*, 2023, 2301148.
7 H. Ye, Y. Peng, X. Shang, L. Li, Y. Yao, X. Zhang, T. Zhu, X. Liu, X. Chen and J. Luo, Self-powered visible–infrared polarization photodetection driven by ferroelectric photovoltaic effect in a Dion–Jacobson hybrid perovskite, *Adv. Funct. Mater.*, 2022, **32**, 2200223.
8 Y. Liu, X. Pan, X. Liu, S. Han, J. Wang, L. Lu, H. Xu, Z. Sun and J. Luo, Tailoring interlayered spacers of two-dimensional cesium-based perovskite ferroelectrics toward exceptional ferro-pyro-phototronic effects, *Small*, 2022, **18**, 2106888.
9 C. Shi, X. Zhang, Y. Cai, Y. Yao and W. Zhang, A chemically triggered and thermally switched dielectric constant transition in a metal cyanide based crystal, *Angew. Chem., Int. Ed.*, 2015, **54**, 6206–6210.
10 Z.-X. Zhang, C.-Y. Su, J. Li, X.-J. Song, D.-W. Fu and Y. Zhang, Ferroelastic hybrid bismuth bromides with dual dielectric switches, *Chem. Mater.*, 2021, **33**, 5790–5799.
11 T. Yang, Y. Liu, L. Hua, Y. Chen, W. Guo, H. Xu, X. Zeng, C. Gao, W. Li, J. Luo and Z. Sun, Lead-free hybrid two-dimensional double perovskite with switchable dielectric phase transition, *Chin. Chem. Lett.*, 2023, 108707.
12 J. Li, C. Xu, W.-Y. Zhang, P.-P. Shi, Q. Ye and D.-W. Fu, Smart and efficient opto-electronic dual response material based on two-dimensional perovskite crystal/thin film, *J. Mater. Chem. C*, 2020, **8**, 1953–1961.
13 S. You, P. Yu, T. Zhu, Q. Guan, J. Wu, H. Dai, H. Zhong, Z.-K. Zhu and J. Luo, Alternating chiral and achiral spacers for constructing two-dimensional chiral hybrid perovskites toward circular-polarization-sensitive photodetection, *Mater. Horiz.*, 2023, **10**, 5307–5312.
14 H. Ye, Y. Peng, M. Wei, X. Zhang, T. Zhu, Q. Guan, L. Li, S. Chen, X. Liu and J. Luo, Bulk photovoltaic effect in chiral layered hybrid perovskite enables highly sensitive near-infrared circular polarization photodetection, *Chem. Mater.*, 2023, **35**, 6591–6597.
15 T. Zhu, W. Weng, C. Ji, X. Zhang, H. Ye, Y. Yao, X. Li, J. Li, W. Lin and J. Luo, Chain-to-layer dimensionality engineering of chiral hybrid perovskites to realize passive highly circular-polarization-sensitive photodetection, *J. Am. Chem. Soc.*, 2022, **144**, 18062–18068.

16 Y. Ma, W. Li, Y. Liu, W. Guo, H. Xu, S. Han, L. Tang, Q. Fan, J. Luo and Z. Sun, Mixing cage cations in 2D metal-halide ferroelectrics enhances the ferro-pyro-phototronic effect for self-driven photopyroelectric detection, *Chem. Sci.*, 2023, **14**, 10347–10352.
17 K. Wang, C. Wu, D. Yang, Y. Jiang and S. Priya, Quasi-two-dimensional halide perovskite single crystal photodetector, *ACS Nano*, 2018, **12**, 4919–4929.
18 I.-H. Park, K. C. Kwon, Z. Zhu, X. Wu, R. Li, Q.-H. Xu and K. P. Loh, Self-powered photodetector using two-dimensional ferroelectric Dion–Jacobson hybrid perovskites, *J. Am. Chem. Soc.*, 2020, **142**, 18592–18598.
19 X. Zeng, Y. Liu, W. Weng, L. Hua, L. Tang, W. Guo, Y. Chen, T. Yang, H. Xu, J. Luo and Z. Sun, A molecular pyroelectric enabling broadband photo-pyroelectric effect towards self-driven wide spectral photodetection, *Nat. Commun.*, 2023, **14**, 5821.
20 L. Lu, W. Weng, Y. Ma, Y. Liu, S. Han, X. Liu, H. Xu, W. Lin, Z. Sun and J. Luo, Anisotropy in a 2D perovskite ferroelectric drives self-powered polarization-sensitive photoresponse for ultraviolet solar-blind polarized-light detection, *Angew. Chem., Int. Ed.*, 2022, **61**, e202205030.
21 W. Guo, H. Xu, W. Weng, L. Tang, Y. Ma, Y. Liu, L. Hua, B. Wang, J. Luo and Z. Sun, Broadband photoresponses from ultraviolet to near-infrared (II) region through light-induced pyroelectric effects in a hybrid perovskite, *Angew. Chem., Int. Ed.*, 2022, **61**, e202213477.
22 M.-Y. Wan, Y.-Z. Tang, Y.-H. Tan, F.-X. Wang, Y.-N. Li, L.-J. Wang, J. Liao and M.-N. Wang, Excellent switchable properties, broad-band emission, ferroelectricity, and high Tc in a two-dimensional hybrid perovskite: $(4,4\text{-DCA})_2PbBr_4$ exploited by H/F substitution, *Inorg. Chem.*, 2023, **62**, 12525–12533.
23 D.-C. Han, Y.-H. Tan, W.-C. Wu, Y.-K. Li, Y.-Z. Tang, J.-C. Zhuang, T.-T. Ying and H. Zhang, High-temperature phase transition containing switchable dielectric behavior, long fluorescence lifetime, and distinct photoluminescence changes in a 2D hybrid $CuBr_4$ perovskite, *Inorg. Chem.*, 2021, **60**, 18918–18923.
24 J. Li, Z.-X. Zhang, T. Zhang, P.-Z. Huang, T. Shao, Y. Zhang and D.-W. Fu, Switchable dielectric two-dimensional lead-free perovskite with reversible thermochromic response, *J. Phys. Chem. C*, 2022, **126**, 16437–16446.
25 Q.-Q. Jia, L. Tong, M.-M. Lun, D.-W. Fu, T. Zhang and H.-F. Lu, Two-dimensional organic–inorganic hybrid materials with dielectric switching and photoluminescence properties, *Cryst. Growth Des.*, 2022, **22**, 2799–2805.
26 C. Qin, L. Xu, Z. Zhou, J. Song, S. Ma, Z. Jiao and Y. Jiang, Carrier dynamics in two-dimensional perovskites: Dion–Jacobson vs. Ruddlesden–Popper thin films, *J. Mater. Chem. A*, 2022, **10**, 3069–3076.
27 S. Ahmad, P. Fu, S. Yu, Q. Yang, X. Liu, X. Wang, X. Wang, X. Guo and C. Li, Dion–Jacobson phase 2D layered perovskites for solar cells with ultrahigh stability, *Joule*, 2019, **3**, 794–806.
28 L. Mao, P. Guo, M. Kepenekian, I. Spanopoulos, Y. He, C. Katan, J. Even, R. D. Schaller, R. Seshadri, C. C. Stoumpos and M. G. Kanatzidis, Organic cation alloying on intralayer A and interlayer A′ sites in 2D hybrid Dion–Jacobson lead bromide perovskites $(A')(A)Pb_2Br_7$, *J. Am. Chem. Soc.*, 2020, **142**, 8342–8351.
29 P. Huang, S. Kazim, M. Wang and S. Ahmad, Toward phase stability: Dion–Jacobson layered perovskite for solar cells, *ACS Energy Lett.*, 2019, **4**, 2960–2974.
30 W.-Q. Wu, Z. Yang, P. N. Rudd, Y. Shao, X. Dai, H. Wei, J. Zhao, Y. Fang, Q. Wang, Y. Liu, Y. Deng, X. Xiao, Y. Feng and J. Huang, Bilateral alkylamine for suppressing charge recombination and improving stability in blade-coated perovskite solar cells, *Sci. Adv.*, 2019, **5**, eaav8925.
31 S. Ahmad, P. Fu, S. Yu, Q. Yang, X. Liu, X. Wang, X. Wang, X. Guo and C. Li, Dion-Jacobson phase 2D layered perovskites for solar cells with ultrahigh stability, *Joule*, 2019, **3**, 794–806.
32 Q. Fan, Y. Ma, S. You, H. Xu, W. Guo, Y. Liu, L. Tang, W. Li, J. Luo and Z. Sun, Dion–Jacobson phase perovskite crystal assembled by π-conjugated aromatic spacer for X-Ray detectors with an ultralow detection limit, *Adv. Funct. Mater.*, 2023, 2312395.
33 Z. Wang, X. Zhang, H. Ye, T. Zhu and J. Luo, A quasi-two-dimensional trilayered $CsPbBr_3$-based Dion Jacobson hybrid perovskite toward high-performance photodetection, *Chem. – Eur. J.*, 2022, **28**, e202200849.
34 B. Wang, H. Chen, W. Guo, Y. Liu, S. Han, L. Hua, L. Tang, J. Luo and Z. Sun, Cage-incorporation of secondary amine in Ruddlesden–Popper 2D hybrid perovskite with strong photoconductivity and polarization response, *J. Mater. Chem. C*, 2021, **9**, 17349–17356.
35 C. Ji, S. Wang, Y. Wang, H. Chen, L. Li, Z. Sun, Y. Sui, S. Wang and J. Luo, 2D hybrid perovskite ferroelectric enables highly sensitive X-Ray detection with low driving voltage, *Adv. Funct. Mater.*, 2020, **30**, 1905529.
36 Y. Li, T. Yang, Z. Xu, X. Liu, X. Huang, S. Han, Y. Liu, M. Li, J. Luo and Z. Sun, Dimensional reduction of Cs2AgBiBr6: A 2D hybrid double perovskite with strong polarization sensitivity, *Angew. Chem., Int. Ed.*, 2020, **59**, 3429–3433.
37 Y. Peng, X. Liu, Z. Sun, C. Ji, L. Li, Z. Wu, S. Wang, Y. Yao, M. Hong and J. Luo, Exploiting the bulk photovoltaic effect in a 2D trilayered hybrid ferroelectric for highly sensitive polarized light detection, *Angew. Chem., Int. Ed.*, 2020, **59**, 3933–3937.
38 D. Fu, W. Jia, S. Wu, J. Chang, Z. Chen and J. Luo, Bilayered Dion–Jacobson hybrid perovskite bulk single crystals constructed with aromatic diammonium for ultraviolet–visible–near-infrared photodetection, *Chem. Mater.*, 2023, **35**, 2541–2548.
39 Q. Fan, Y. Ma, H. Xu, Y. Liu, B. Wang, W. Guo, X. Hu, J. Luo and Z. Sun, Acquiring a newly tailored 2D Dion–Jacobson hybrid perovskite with large structural distortion for efficient crystal array photodetector, *Adv. Opt. Mater.*, 2023, **11**, 2202277.